Terminal Velocities of Droplets and Crystals: Power Laws with Continuous Parameters over the Size Spectrum

VITALY I. KHVOROSTYANOV

Central Aerological Observatory, Dolgoprudny, Moscow, Russia

JUDITH A. CURRY

Department of Aerospace Engineering Sciences, University of Colorado, Boulder, Boulder, Colorado

(Manuscript received 16 March 2001, in final form 23 October 2001)

ABSTRACT

This paper presents a unified treatment of cloud particle fall velocities for both liquid and crystalline cloud particles over the entire size range observed in the atmosphere. The fall velocity representation is formulated in terms of the Best (or Davies) number X, and the Reynolds number Re. For the power-law representations used in many applications, the coefficients are found as the continuous analytical functions of X (or diameter) over the entire hydrometeor size range. Analytical asymptotic solutions are obtained for these coefficients for the two regimes that represent large and small particles and correspond to potential and aerodynamical flows, respectively. The new formulation is compared with experimental data and previous formulations for small drops, large nonspherical drops, and various ice crystal habits. For ice crystals, published mass–dimension and area–dimension relationships are used. The advantage of the new representation of fall velocities over previous representations is that the continuous representation avoids inaccuracy at the points of discontinuity for different size regimes, allows easier parameterization of the hydrometeor size spectra, and allows for continuous integration over the size spectrum. The new fall velocity formulation may be applied to bin-resolving and bulk microphysical models, as well as to remote sensing.

1. Introduction

Accurate parameterization of gravitational settling and fallout of cloud particles and hydrometeors is essential for accurate simulation by cloud and general circulation models (GCMs) of precipitation amount, cloud dissipation, and cloud optical properties. Problems in parameterization of the fallout of cirrus cloud particles have been highlighted by the Intercomparison of the Cirrus Cloud and Parcel Models Projects performed within the Working Group 2 on Cirrus Clouds of the Global Energy and Water Cycle Experiment (GEWEX) Cloud System Study (GCSS; Randall et al. 2002, in preparation). These intercomparisons showed large differences in calculated ice crystal terminal velocities among similar models and illustrated the high sensitivity of the simulated cloud properties to the parameterization of fall velocity (Starr et al. 2000; Lin et al. 2000). The intercomparisons stimulated a special activity on the sensitivity and comparison studies of the fall velocities (P. Brown 1998, personal communication; see http://eos913c.gsfc.nasa.gov/gcss_wg2/). Recent numerical experiments with single column models (Petch et al. 1997) and with the European Centre for Medium-Range Weather Forecasts (ECMWF) model (Miller and Stephens 2001; Heymsfield and Iaquinta 2000) showed that relatively small variations in parameterized ice crystal terminal velocities produce substantial differences in the simulated ice water paths, cloud boundaries and cloud optical properties. This led to the conclusion that the discrepancies between the GCM-produced and satellite-measured global radiative balance can be caused by inaccurate parameterization of fall velocities.

Whereas a number of factors can contribute to inaccurate simulation of the gravitational fallout of cloud particles and hydrometeors (e.g., inaccuracies in parameterization of particle size distribution, habit, and density), a key element in the parameterization of gravitational fallout of cloud particles and hydrometeors is the terminal velocity. Previous experimental studies have produced a wealth of data on terminal velocities, which are typically parameterized in the form of power laws:

$$V_t = A_v D^{B_v}, \tag{1.1}$$

where V_t is the terminal velocity, D is the particle di-

Corresponding author address: Dr. J. A. Curry, Department of Aerospace Engineering Sciences, UCB 429, University of Colorado, Boulder, CO 80309-0429.
E-mail: curryja@cloud.colorado.edu

ameter or maximum length, and the coefficients A_v and B_v are determined from best fits to the experimental data (e.g., Gunn and Kinzer 1949; Litvinov 1956; Bashkirova and Pershina 1964; Jayaweera and Cottis 1969; Heymsfield 1972; Locatelli and Hobbs 1974, hereafter LH74; Beard 1976; Heymsfield and Kajikawa 1987; Mitchell 1994; Mitchell and Arnott 1994). A universal dependence of V_t in the form (1.1) has not been found since the coefficients vary over the size spectrum; however, several fits to the experimental data have been given with A_v, B_v constant over some subranges of the size spectrum. For example, Rogers (1976), based on the data of Gunn and Kinzer (1949), gave the following approximation for liquid drops of radius r:

$$V_t = k_1 r^2, \qquad 0 < r < 40\ \mu\text{m}, \tag{1.2a}$$

$$V_t = k_2 r, \qquad 40\ \mu\text{m} < r < 600\ \mu\text{m}, \tag{1.2b}$$

$$V_t = k_3 r^{1/2}, \qquad r > 600\ \mu\text{m}, \tag{1.2c}$$

with $k_1 = 1.19 \times 10^6\ \text{cm}^{-1}\ \text{s}^{-1}$, $k_2 = 8 \times 10^3\ \text{s}^{-1}$, and $k_3 = 2.2 \times 10^3\ (\rho_{a0}/\rho_a)^{1/2}\ \text{cm}^{1/2}\ \text{s}^{-1}$. Similar parameterizations have been developed for ice crystals; for example, Starr and Cox (1985a,b) found the best fit for cirrus cloud particles using five subregions of the size spectrum with different coefficients. Parameterizations of the power-law type (1.1), (1.2) are used in many cloud models, general circulation models, and remote sensing techniques; however, attempts to derive these coefficients theoretically are scarce.

Stokes developed in 1851 the theory of fall velocities for spherical drops in a laminar viscous flow at small Reynolds numbers. Numerous attempts have been made to extend this theory for larger values of the Reynolds number and nonspherical drops and crystals. However, a general theory remained elusive for a long time because flow around a particle and its turbulent wake are complicated and evolve with increasing values of the Reynolds number. The nonsphericity of a hydrometeor further complicates the flow. Some sophisticated numerical models based on the solution of the Navier–Stokes equations have been applied to study the stream functions and vorticity of the turbulent flow around the objects of the simplest shapes: spheres, spheroids, circular cylinders (for a review, see Pruppacher and Klett 1997, hereafter PK97). However, such models have not been successfully used to develop simple parameterizations like (1.1) that can be used in numerical cloud models and GCMs.

Substantial progress in finding a simple but general solution to the fall velocity problem was made by Abraham (1970). He showed that fluid motion around a rigid sphere can be divided into two regions: 1) a region close to the object where frictional effects are important; and 2) an outer region where friction may be neglected. The first regime corresponds to the viscous flow around the body with maximum projected cross-sectional area A and the drag force $F_D(A) = (1/2)C_D\rho_F V_t^2 A$, where C_D is the drag coefficient, and ρ_F is the fluid density. Abraham (1970) suggested considering the second regime as the assembly of the body and the boundary layer with total projected area A_t so that the assembly moves in a potential flow with the drag force $F_{D0}(A_t) = (1/2)\ C_0\rho_F V_t^2 A_t$, where C_0 is the drag coefficient for the potential flow around the assembly without friction. Matching these two regimes, Abraham found a general functional dependence of the drag on Reynolds number.

The next significant step was made by Bohm (1989, 1992) who used Abraham's model of the flow around a falling particle to determine a general analytical relation between the Reynolds number Re, and Best (or Davies) number $X = C_D\text{Re}^2$. Then, inverting the definition of Re, Bohm obtained a general expression for V_t as a function of X. Bohm's X–Re relations are algebraic functions that are more complicated than the power law (1.1). Mitchell (1996) extended Bohm's work, found a power-law representation for the X–Re relationship for four different regimes of X over the range $0.01 < X < 10^8$, and derived power-law expressions for the fall velocities of nonspherical ice crystals using experimental mass–dimension (m–D) and area–dimension (A–D) relations. Mitchell's formulation leads to a convenient power-law representation of $V_t(D)$. Heymsfield and Iaquinta (2000), based on Mitchell's Re–X power law, expressed V_t in terms of the (m–A) relation, and developed parameterizations of the fall velocities for some crystal types in cirrus.

A disadvantage of Mitchell's (1996) and other previous formulations is that, although the fall velocities themselves are continuous functions of the particle diameter D, the coefficients in power-law relations of the type (1.1) are stepwise functions of X (or D), and the derivative dV_t/dD is discontinuous at the matching points. A continuous representation of the X–Re relationship or of the coefficients in (1.1) is desired for several reasons:

1) a continuous representation eliminates the inaccuracies introduced at the boundaries of the several different X regimes;
2) many numerical models and remote sensing techniques use the power-law representation of V_t and require a continuous integration over the size spectrum when evaluating its moments (e.g., Matrosov and Heymsfield 2000), and this is easier and more accurate with coefficients that are continuous over the entire size spectrum;
3) in some spectral bin models, the numerical schemes for evaluation of the size distribution function $f(D)$ or mass function $f(m)$ are based on derivatives with respect to particle size [e.g., $d(fV_t)/dD$] and discontinuities at the matching points produce numerical errors;
4) an analytical solution to the kinetic equation for $f(D)$ in the form of a gamma distribution was obtained for the falling particles with fall velocity of the pow-

er-law type (Khvorostyanov and Curry 1999a,b); an analysis of the solution showed that these coefficients should be continuous functions of D.

Such a continuous form of the coefficients in power laws for the Re–X relations and for fall velocities is found in this paper. The new formulation is compared with experimental data and previous formulations for small drops, large nonspherical drops, and various ice crystal habits. Applications of the new fall velocity formulation to bin and bulk microphysical models and remote sensing are discussed.

2. Theoretical formulation

The formulation developed here extends the works of Bohm (1989, 1992) and Mitchell (1996), which in turn are based on the paper by Abraham (1970). The drag force around a rigid sphere of radius r is obtained by matching the drag forces for these two regions following Abraham (1970), as described in the previous section:

$$F_D = (1/2)C_D\rho_F V_t^2 A = F_{D0} = (1/2)C_0\rho_F V_t^2 A_t. \quad (2.1)$$

The total projected area A_t for a sphere of radius r according to Abraham (1970) is related to the sphere of radius r and the boundary layer depth δ:

$$A_t = \pi(r + \delta)^2 = \pi r^2(1 + \delta/r)^2 \quad (2.2)$$

Introducing Reynolds number $\mathrm{Re} = V_t D/\nu = V_t D\rho_F/\eta$, where $D = 2r$ is the sphere diameter, ν is the fluid kinematic viscosity (related to the dynamic viscosity η and fluid density ρ_F as $\nu = \eta/\rho_F$), and the depth δ is determined from boundary layer theory through

$$\frac{\delta}{r} = \frac{\delta_0}{\mathrm{Re}^{1/2}}. \quad (2.3)$$

Substitution of (2.2) and (2.3) into (2.1), gives the drag coefficient as in Abraham (1970):

$$C_D = C_0(1 + \delta_0/\mathrm{Re}^{1/2})^2. \quad (2.4)$$

The constants C_0 and δ_0 were determined by Abraham to be $C_0 = 0.29$ and $\delta_0 = 9.06$. Using these values in (2.4), the limiting value of C_D at low Re is determined to be $C_D = C_0\delta_0^2/\mathrm{Re} = 24/\mathrm{Re}$, which is the well-known expression for drag in the Stokes regime. These values of C_0 and δ_0 give an intermediate solution at $\mathrm{Re} > 1$ between the Stokes solution (which underestimates the drag) and Oseen's solution to the Navier–Stokes equations (which overestimate C_D) and provide excellent agreement with experimental data.

The terminal velocity V_t of a falling body is obtained by equating the drag force F_D to the difference of the gravitational force $mg = \rho_b \mathrm{v}_b g$ and the buoyancy force $F_b = \rho_F \mathrm{v}_b g$:

$$mg - F_b = (\rho_b - \rho_F)\mathrm{v}_b g = F_D = (1/2)C_D\rho_F V_t^2 A, \quad (2.5)$$

where ρ_b is the body density, v_b is its volume, and g is the acceleration of gravity. Solving for V_t, we obtain

$$V_t = \left[\frac{2[|mg - F_b|]}{\rho_F A C_D}\right]^{1/2} = \left[\frac{2g\mathrm{v}_b|\rho_F - \rho_b|}{C_D A\rho_F}\right]^{1/2}. \quad (2.6)$$

The new dependence of C_D on V_t complicates the solution of (2.6). The problem is usually solved by introducing the Davies or Best number X:

$$X = C_D\mathrm{Re}^2 = \frac{2(mg - F_b)\rho_F D^2}{A\eta^2} = \frac{2\mathrm{v}_b(\rho_b - \rho_F)gD^2}{A\rho_F\nu^2}, \quad (2.7)$$

where D is the maximum dimension of the body (particle). The drag coefficient C_D can then be determined as a function of Re and X, which is a parameter that depends only on physical variables. To derive a continuous X–Re relationship and hence a continuous expression for V_t, we proceed as follows. Substitution of (2.4) into (2.7) leads to a quadratic equation, the positive root giving Bohm's (1989) X–Re relation:

$$\mathrm{Re} = (\delta_0^2/4)[(1 + c_1X^{1/2})^{1/2} - 1]^2, \quad (2.8)$$

where we have introduced the constant $c_1 = 4/(\delta_0^2C_0^{1/2}) = 0.0902$. Bohm's relation [(2.8)] is not a power law, but it can be presented as one polynomial:

$$\mathrm{Re} = a_{\mathrm{Re}}X^{b_{\mathrm{Re}}}. \quad (2.9)$$

Mitchell (1996) found the best numerical fits for a_{Re}, b_{Re} in four X intervals.

We will find now a representation for the coefficients a_{Re} and b_{Re} as continuous, smooth functions of X in the entire X range as follows. Consider a continuous function $\varphi(X)$ with continuous derivative $\varphi'(X)$. This function can be represented in a power-law form as $\varphi(X) = aX^b$, so its derivative $\varphi'(X) = abX^{b-1}$. Solving these two equations, the coefficients a, b can be expressed via φ, φ' as

$$b = X(\varphi'/\varphi), \quad \text{and} \quad a = \varphi/X^b. \quad (2.10)$$

For the terminal velocity application, $\varphi(X) = \mathrm{Re}(X)$, and we can write, using (2.8),

$$\varphi'(X) = \mathrm{Re}'(X) = \frac{1}{2C_0^{1/2}}[(1 + c_1X^{1/2})^{1/2} - 1] \times (1 + c_1X^{1/2})^{-1/2}X^{-1/2}. \quad (2.11)$$

Substituting (2.8) and (2.11) into (2.10), we obtain the following expressions for a_{Re}, b_{Re}:

$$b_{\mathrm{Re}}(X) = \frac{1}{2}c_1X^{1/2}[(1 + c_1X^{1/2})^{1/2} - 1]^{-1} \times (1 + c_1X^{1/2})^{-1/2}, \quad \text{and} \quad (2.12)$$

$$a_{\mathrm{Re}}(X) = (\delta_0^2/4)[(1 + c_1X^{1/2})^{1/2} - 1]^2/X^{b_{\mathrm{Re}}(X)}. \quad (2.13)$$

Equations (2.12) and (2.13) provide a power-law rep-

resentation of $\mathrm{Re}(X)$ with a_{Re}, b_{Re} being continuous functions of X that are consistent with the X–Re relation (2.8).

It is useful to find the asymptotic values of these coefficients since they define the limiting behavior of the fall velocities. It is seen from (2.12) and (2.13) that the asymptotic values of a_{Re}, b_{Re} are reached at $c_1X^{1/2} \ll 1$, and $c_1X^{1/2} \gg 1$. Hence we can introduce the scaling Best parameter from the condition $c_1X_{\mathrm{sc}}^{1/2} = 1$, or $X_{\mathrm{sc}} = 1/c_1^2 = 123$. The value of X_{sc} separates the two regimes for small and large particles (or, as will be shown later, the regimes of potential and aerodynamical flows). For $X \ll X_{\mathrm{sc}}$, we find from (2.12) and (2.13) by expanding into the power series,

$$b_{\mathrm{Re}}(X) \approx (1/2)c_1X^{1/2}[(1/2)c_1X^{1/2}]^{-1} = 1, \quad \text{and} \tag{2.14}$$

$$a_{\mathrm{Re}}(X) \approx (\delta_0^2/4)[(1/2)c_1X^{1/2}]^2X^{-1} = 1/(C_0\delta_0^2) = 0.0417. \tag{2.15}$$

These values are in a good agreement with Mitchell's (1996) fit $a_{\mathrm{Re}} = 0.0439$, $b_{\mathrm{Re}} = 0.97$ in the range $X = 0.01$–10 and not very far from his values $a_{\mathrm{Re}} = 0.06049$, $b_{\mathrm{Re}} = 0.831$, at $X = 10$–585, although our limit is valid only for $X \ll X_{\mathrm{sc}}$. For $X \gg X_{\mathrm{sc}}$, it follows from (2.12) and (2.13) that

$$b_{\mathrm{Re}} = (1/2)c_1X^{1/2}(c_1X^{1/2})^{-1} = 1/2, \quad \text{and} \tag{2.16}$$

$$a_{\mathrm{Re}} = (\delta_0^2/4)(c_1X^{1/2})X^{-1/2} = 1/C_0^{1/2} = 1.85. \tag{2.17}$$

The limiting value of b_{Re} is very close to the Mitchell's (1996) fit $b_{\mathrm{Re}} = 0.499$ at $1.56 \times 10^5 < X < 10^8$, while our limit of a_{Re} is larger than Mitchell's $a_{\mathrm{Re}} = 1.0865$. An expression that relates the scaling body dimension D_{sc} (which separates the two limiting regimes) to X_{sc} can be obtained by inverting (2.7):

$$D_{\mathrm{sc}} = \left[X_{\mathrm{sc}}\frac{A\rho_F\nu^2}{2(mg - F_b)}\right]^{1/2}. \tag{2.18}$$

The drag coefficient can be determined using (2.7) and (2.9) to be

$$C_D = \frac{X}{\mathrm{Re}^2} = a_{\mathrm{Re}}^{-2}X^{1-2b_{\mathrm{Re}}} = a_{\mathrm{Re}}^{-2}\left[\frac{2(mg - F_b)\rho_F D^2}{A\eta}\right]^{1-2b_{\mathrm{Re}}}. \tag{2.19}$$

Substitution of (2.19) into (2.6) yields the following expression for the terminal velocity:

$$V_t = a_{\mathrm{Re}}\nu^{1-2b_{\mathrm{Re}}}\left[\frac{2(mg - F_b)}{\rho_F A}\right]^{b_{\mathrm{Re}}} D^{2b_{\mathrm{Re}}-1} \tag{2.20a}$$

$$= a_{\mathrm{Re}}\nu^{1-2b_{\mathrm{Re}}}\left[\frac{2\mathrm{v}_b g}{A}\left(\frac{\rho_b - \rho_F}{\rho_F}\right)\right]^{b_{\mathrm{Re}}} D^{2b_{\mathrm{Re}}-1}. \tag{2.20b}$$

It is assumed above that $\rho_b > \rho_F$, but the density difference in (2.20b) should be $(\rho_F - \rho_b)$ in the reverse cases that are discussed below. In many applications, objects can be approximated by ellipsoids of specified axis ratio $\xi(D)$, then $\mathrm{v}_b = (\pi/6)D^3\xi(D)$, $A = (\pi/4)D^2$, and $\mathrm{v}_b/A = (2/3)D\xi(D)$. Then,

$$V_t = a_{\mathrm{Re}}\nu^{1-2b_{\mathrm{Re}}}\left[\frac{4}{3}g\xi(D)\left(\frac{\rho_b}{\rho_F} - 1\right)\right]^{b_{\mathrm{Re}}} D^{3b_{\mathrm{Re}}-1}. \tag{2.20c}$$

The equations derived above are valid for various ''liquids'' and bodies. In applications for falling hydrometeors in the earth's atmosphere, we consider air as the ''fluid'' and a drop or a crystal as the ''body''; henceforth, we use ρ_a (density of air) in place of ρ_F, and ρ_b denotes the density of drops or crystals. We can use relationships for the particle mass and cross-sectional area to be a function of diameter as (following Mitchell 1996 and others),

$$m = \alpha D^\beta, \quad \text{and} \quad A = \gamma D^\sigma. \tag{2.21}$$

where α, β, γ, σ vary with particle size, phase, and habit. Using (2.21), D_{sc} is expressed as

$$D_{\mathrm{sc}} = \left(X_{\mathrm{sc}}\frac{\gamma\rho_a\nu^2}{2\alpha g}\right)^{1/(\beta-\sigma+2)}. \tag{2.22}$$

Incorporating the relations in (2.21) into (2.20a) and neglecting F_b compared to mg (since $\rho_a \ll \rho_b$), we obtain

$$V_t = A_\upsilon D^{B_\upsilon}, \tag{2.23}$$

where the coefficients are

$$A_\upsilon = a_{\mathrm{Re}}\nu^{1-2b_{\mathrm{Re}}}\left(\frac{2\alpha g}{\rho_a\gamma}\right)^{b_{\mathrm{Re}}}, \quad \text{and} \tag{2.24}$$

$$B_\upsilon = b_{\mathrm{Re}}(\beta - \sigma + 2) - 1. \tag{2.25}$$

Expressions (2.23)–(2.25) are the same as in Mitchell (1996); however, since the coefficients a_{Re} and b_{Re} are given in (2.12) and (2.13) as continuous functions of X, (2.23) to (2.25) give a continuous power-law representation of the terminal velocity over the entire particle size range. Note that the factor $\nu^{1-2b_{\mathrm{Re}}}$ in (2.24) for A_υ, along with the asymptotic value for b_{Re}, describes the correct dependence of V_t on viscosity: for small particles, $b_{\mathrm{Re}} = 1$, and $1 - 2b_{\mathrm{Re}} = -1$, so $V_t \sim \nu^{-1}$ (viscous Stokes regime); while for the large drops, $b_{\mathrm{Re}} = 0.5$, and $1 - 2b_{\mathrm{Re}} = 0$, so V_t is independent of viscosity as should be in an aerodynamic regime.

The dependence of fall velocities on temperature and pressure can be determined using the equation of state $p = \rho_a RT$, and substituting ρ_a as a function of T, p into (2.24). This yields

$$V_t(p, T) = c_{pT}V_t(p_0, T_0), \quad \text{and} \quad c_{pT} = \left(\frac{p_0}{p}\frac{T}{T_0}\right)^{b_{\mathrm{Re}}}, \tag{2.26}$$

where $V_t(p_0 = 1000\ \mathrm{hPa}, T_0 = 293\ \mathrm{K})$ is calculated

TABLE 1. Coefficients of mass and area power laws for drops and crystals used in calculations of a_v, b_v. Those for crystals are from Mitchell (1996) with some data from Locatelli and Hobbs (1974), Heymsfield and Kajikawa (1987), and Heymsfield and Iaquinta (2000).

Particle type	Mass		Area		Remark
	α	β	γ	σ	
Speherical drops	$(\pi/6)\rho_w = 0.524$	3	$\pi/4 = 0.785$	2	
Nonspherical drops	$(\pi/6)\rho_w \times \zeta(D)$	3	$\pi/4 = 0.785$	2	
Hexagonal plates (Pla)					
15 μm $< D <$ 100 μm	0.00739	2.45	0.24	2.00	$\alpha = 0.0376$, $\beta = 3.31$, $A_v = 297$, $B_v = 0.86$ (HK87)
100 μm $< D <$ 3000 μm	0.00739	2.45	0.65	1.85	
Hexagonal Columns					
30 μm $< D <$ 100 μm	0.1677	2.91	0.684	2.00	
100 μm $< D <$ 300 μm	0.00166	1.91	0.0696	1.50	
$D >$ 300 μm	0.000907	1.74	0.0512	1.414	
Rimed long columns					
200 μm $\leq$ 2400 μm	0.00145 (old) 0.00125 (new)	1.8	0.0512	1.414	
Crystal with sector-like brances (P1b)					
10 μm $< D <$ 40 μm	0.00614	2.42	0.24	1.85	
40 μm $< D <$ 2000 μm	0.00142	2.02	0.55	1.97	
Broad-branched crystal (P1c)					
10 μm $< D <$ 100 μm	0.00583	2.42	0.24	1.85	
100 μm $< D <$ 1000 μm	0.000516	2.02	0.21	1.76	
Stellar crystal with broad arms (P1d)					
10 μm $< D <$ 90 μm	0.00583	2.42	0.24	1.85	
90 μm $< D <$ 1500 μm	0.00027	1.67	0.11	1.63	
Densely rimed dendrites (R2b)					
1800 μm $< D <$ 4000 μm	0.030 (old) 0.015 (new)	2.3	0.21	1.76	$A_v = 62$, $B_v = 0.33$ (LH74)
Bullet rosettes, five branches					
200 μm $< D <$ 1000 μm	0.00308	2.26	0.0869	1.57	$A_v = 2150$, $B_v = 1.225$ ($D <$ 0.06 cm) $A_v = 492$, $B_v = 0.7$ ($D >$ 0.06 cm) (Heymsfield and Iaquinta 2000)

using (2.24) and ρ_{a0} under standard conditions ($\rho_{a0} = 1.23 \times 10^{-3}$ g cm^{-3}), while the correction c_{pT} determines the p–T dependencies and b_{Re} can be calculated from (2.14). The values of c_{pT} can be illustrated by an example of comparison of V_t at sea level ($p = 1000$ hPa, $T = 293$ K) and at cirrus altitude ($p = 400$ hPa, $T = 223$ K). Substituting these values into (2.26), we obtain for small particles ($b_{\mathrm{Re}} = 1$) an estimation of $c_{pT} = 1.95$, and for large particles ($b_{\mathrm{Re}} = 0.5$), $c_{pT} = 1.4$. Thus, small crystals at 400 mb fall twice as fast as at sea level, while large particle at high altitude fall only 40% faster. The difference in fall velocities becomes smaller, hampering the coagulation processes with increasing height.

3. Results

This section evaluates the coefficients a_{Re}, b_{Re}, the X–Re relationships, and the terminal velocities for drops of different sizes and crystals of different sizes and habits. A comparison is made with previous formulations and also with experimental data. The coefficients A_v, power indices B_v, and fall velocities for the various particles were calculated using the following method: 1) the four coefficients α_i, β_i, γ_i, and σ_i were prescribed for each ith particle type [the coefficients are given in Table 1, those for crystals are taken from Mitchell (1996)]; 2) using these coefficients, the parameter X_i was calculated for each particle type from (2.7); 3) the coefficients $a_{\mathrm{Re},i}$ and $b_{\mathrm{Re},i}$ were calculated from (2.12) and (2.13) as the functions of X_i, that is, of D_i; and 4) the coefficients A_v, B_v, and V_t were calculated using (2.23)–(2.25) as the functions of D_i.

a. Spherical drops, graupel, and hail

In this section, we consider spherical particles, including drops, graupel, and hail. For simplicity we examine primarily drops using the water density ρ_w, however, the same equations are valid for spherical graupel and hail after replacing ρ_w with ice density ρ_i (which may depend also on D). For spherical drops, the mass and area are related to the diameter by $m = (\pi/6)\rho_w D^3$ and $A = (\pi D^2/4)$; thus from (2.21) we find that $\alpha = (\pi/6)\rho_w$, $\beta = 3$, $\gamma = \pi/4$, $\sigma = 2$. Substituting these values into (2.24) and (2.25), we obtain the following expression for spherical particles:

$$A_v = a_{\mathrm{Re}} \nu^{1-2b_{\mathrm{Re}}} \left(\frac{4}{3} \frac{\rho_w g}{\rho_a} \right)^{b_{\mathrm{Re}}}, \qquad B_v = 3b_{\mathrm{Re}} - 1. \quad (3.1)$$

This expression can be evaluated for small and large

drops using the scaling diameter from (2.18), which yields (under standard atmospheric conditions) $D_{sc} = 134\ \mu$m.

For small droplets ($D < D_{sc}$), using the asymptotic values given above, $a_{Re} = 1/(C_0\delta_0^2)$ and $b_{Re} = 1$ from (2.14) and (2.15), we obtain V_t in terms of radius r as

$$V_t(r) = A_v(2r)^{B_v} = A_{vr}r^{B_v}, \quad \text{with}$$

$$A_{vr} = 2^{B_v}A_v = \frac{16\rho_w g}{3\delta_0^2 C_0 \rho_a \nu}, \qquad B_v = 2. \quad (3.2)$$

This expression is consistent with Stokes law for the viscous regime $V_t \sim r^2$. The coefficient A_{vr} is similar to that obtained by Mitchell (1996), except that it includes δ_0, C_0 instead of a numerical constant based on the fit in Mitchell (1996). Using $\delta_0 = 9.06$, $C_0 = 0.292$ gives $A_{vr} = 1.2 \times 10^6\ \text{cm}^{-1}\ \text{s}^{-1}$, that is, the Stokes constant.

For large droplets, ($D > D_{sc}$), $a_{Re} = 1.85$ and $b_{Re} = 0.5$ are evaluated from (2.16), (2.17), and

$$A_{vr} = 2^{1/2}A_v = 2^{1/2}a_{Re}\left(\frac{4}{3}\frac{\rho_w g}{\rho_a}\right)^{1/2}, \qquad B_v = 0.5. \quad (3.3)$$

So, $V_t \sim r^{1/2}$, as it should be for spherical particles in aerodynamic regime when C_D does not depend on V_t and as is seen from (2.6) (see also, e.g., Cotton and Anthes 1989). Evaluation of the coefficient gives $A_{vr} = 2.72 \times 10^3\ \text{cm}^{1/2}\ \text{s}^{-1}$, which is higher than the corresponding value of $2.2 \times 10^3\ \text{cm}^{1/2}\ \text{s}^{-1}$ given in Rogers (1976) based on experimental data [see Eq. (1.2c)]. The disagreement of (3.3) with experimental data arises because the nonsphericity of falling drops has not been considered but is partially accounted for by Rogers (these effects are considered in section 3b).

b. Nonspherical large drops

The nonsphericity of the drops becomes substantial for the fall velocity at $D > 535\ \mu$m (PK97). Large falling drops have shapes that can be approximated by an oblate spheroid with maximum diameter D oriented perpendicular to the flow and the smaller diameter D_s is oriented vertically. Measurements and models described in PK97 show that the aspect ratio $\xi = D_s/D = 1$ for small drops and decreases with D. We approximate aspect ratio with the interpolation formula,

$$\xi(D) = \exp\left(-\frac{D}{\lambda}\right) + \left[1 - \exp\left(-\frac{D}{\lambda}\right)\right]\left[\frac{1}{1 + (D/\lambda)}\right]. \quad (3.4)$$

This equation ensures decrease of $\xi(D)$ with increasing D and satisfies the condition $\xi = 1$ at $D \to 0$. The parameter λ was found from the condition $\xi = 0.5$ at $D \sim 8.5$ mm, after which drop breakup occurs due to hydrodynamic instability (PK97). With this condition,

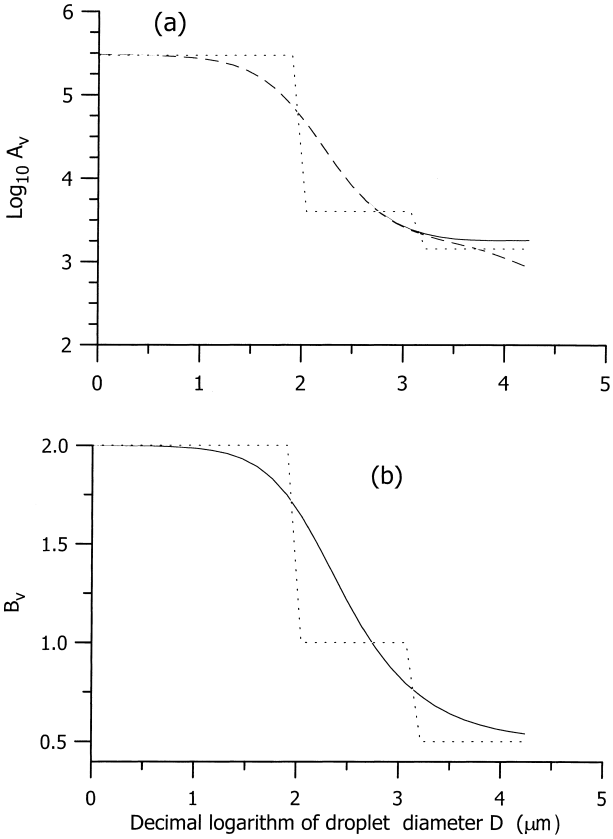

FIG. 1. Comparison of the coefficients (2.23), (2.24) of the velocity power law (2.23) (solid), with Rogers' (1976) stepwise formulation (1.2) for the spherical drops (dot) and oblate spheroids (dash): (a) A_v (2.24); (b) B_v (2.25).

$\lambda = 4.7$ mm. Considering the large drop as an ellipsoid, we obtain from (2.21) $\alpha(D) = (\pi/6)\rho_w\xi(D)$, $\beta = 3$, $\gamma = \pi/4$, and $\sigma = 2$. Using (2.23)–(2.25) and asymptotics at large D, $b_{Re} = 0.5$ from (2.18) and $\xi(D) \sim D^{-1}$ from (3.4), we obtain for large D,

$$V_t(D) \sim \alpha^{b_{Re}}D^{b_{Re}(\beta-\sigma+2)} \sim \xi(D)^{b_{Re}}D^{b_{Re}(\beta-\sigma+2)} \sim D^{-0.5}D^{0.5} \sim D^0. \quad (3.5)$$

So, V_t is asymptotically independent on D with $\xi(D)$ in (3.4). This is in agreement with observations of Gunn and Kinzer (1949) that show very weak dependence of V_t on the drop size at $D > 4$–5 mm (see Fig. 2 below).

Figure 1 compares the coefficients A_v, B_v for the drops calculated using (2.24) and (2.25) with Rogers' (1976) stepwise parameterization. Note that the new curves look like smoothing fits to Rogers' line segments. Figure 2 compares the fall velocities for liquid drops up to 8.5 mm using the new formulation, the data from Gunn and Kinzer (1949), and the piecewise formulation of Rogers (1976). This figure shows that: 1) the effects of nonsphericity become significant at $D > 2$ mm; 2) Rogers' parameterization overestimates V_t as compared to Gunn and Kinzer (1949) data at $D > 4$ mm; 3) the new for-

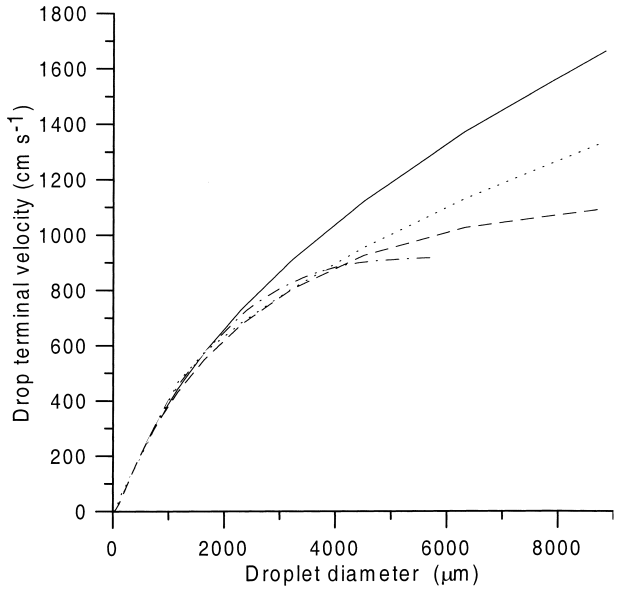

FIG. 2. Drop terminal velocities (under standard atmospheric conditions), determined using the new formulation for spherical drops (S, solid), oblate ellipsoids as described in the text (OE, dash), Roger's (1976) formulation (R76, dot), and observations of Gunn and Kinzer (1949) (GK49, dot–dash).

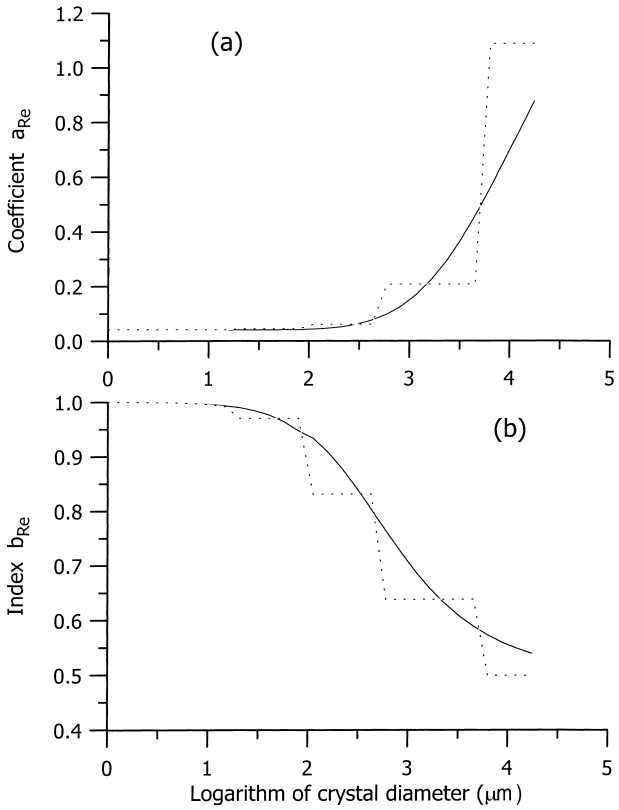

FIG. 3. Comparison of the new formulation for the coefficients in the X–Re relationship (2.12), (2.13) (solid) with Mitchell's (1996) stepwise formulation (dot) for the hexagonal plates: (a) a_{Re} and (b) b_{Re}.

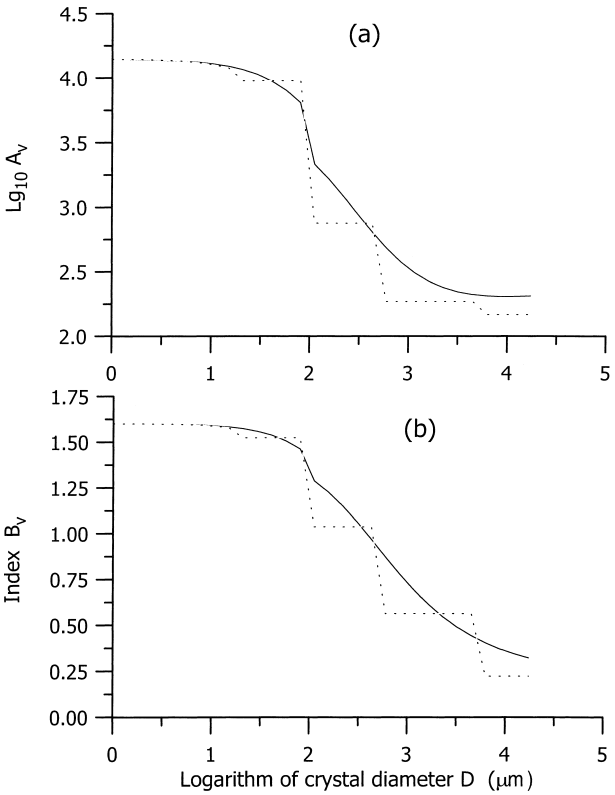

FIG. 4. Comparison of the coefficients of the velocity power law (2.23) (solid) for hexagonal plates with Mitchell's (1996) stepwise formulation (dot): (a) A_v (2.24); (b) B_v (2.25).

mulation for nonspherical drops with aspect ratio (3.4) exhibits slower increase of V_t with D (independence on D at larger sizes) and produces a closer agreement with the observational data.

c. Ice crystals

Figure 3 compares the coefficients in the X–Re relationship determined from the new formulation with Mitchell's (1996) stepwise formulation for hexagonal plates (P1a, according to Magono and Lee 1966). Figure 4 compares the coefficients of the velocity power law (2.23) determined from the new formulation with Mitchell's stepwise formulation. These figures illustrate that the continuous functions (2.12), (2.13) and (2.24), (2.25) provide similar values to Mitchell's stepwise functions, but avoid the substantial discontinuities present in the stepwise formulation. Note that although a_{Re} and b_{Re} are smooth functions of D over the entire size region (Fig. 3), discontinuity of the curves is still seen at $D = 100$ μm, which is caused by the changing coefficients $\alpha(D)$, $\beta(D)$, $\gamma(D)$, and $\sigma(D)$ in (2.24), (2.25). These coefficients in the m–D and A–D relations are usually determined as empirical fits in various D regions (see Table 1). It is not clear if discontinuity arises from the measurements of the crystal properties by different devices

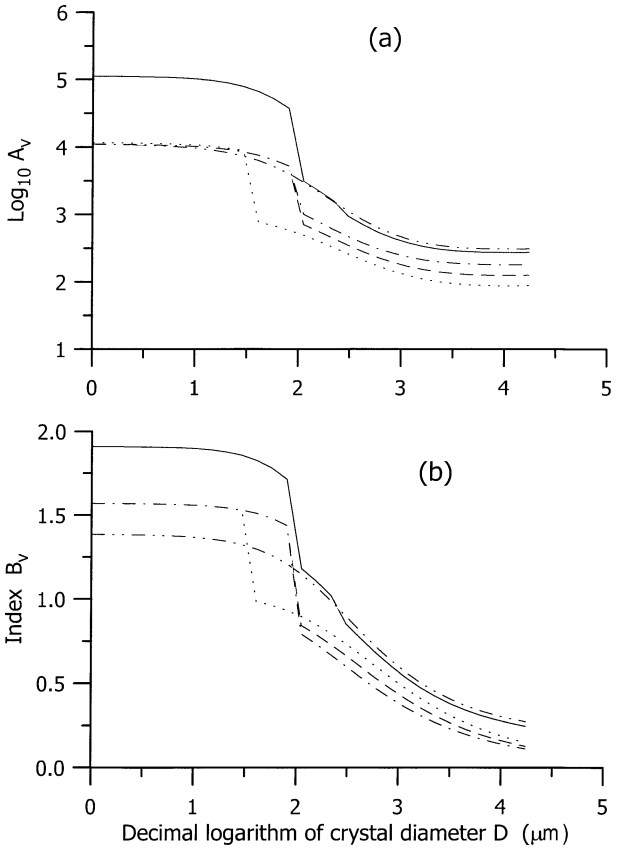

FIG. 5. Comparison of the coefficients of the velocity power law (2.23) for various crystal habits: hexagonal columns (solid), plate with sector branches (dot), rimed columns (dot–dash–dot), plate with broad branches (dash), stellar dendrites (dot–dash): (a) A_v; (b) B_v.

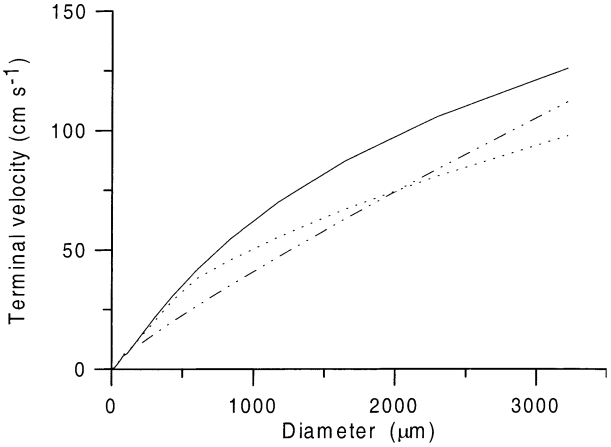

FIG. 6. Comparison of terminal velocities for hexagonal plates (P1a) under standard atmospheric conditions determined using the new formulation (solid), Mitchell's (1996) stepwise formulation (dot), and the experimental data of Heymsfield and Kajikawa (1987; dash–dot–dot).

in various size regions [e.g., forward-scattering spectrometer probe (FSSP) and (2DC)], deficiency of the empirical parameterizations, or if this variation in coefficients is caused by the acceleration of accretion processes at $D > 100$ μm. In any case, development of *m–D* and *A–D* relations that are continuous in the entire size interval is desired.

The influence of habit on the coefficients A_v, B_v used in the power-law representation of V_t (2.23) is shown in Fig. 5 for the following different ice crystal habits: hexagonal columns (C1f), plates with sector branches (P1b), rimed columns, plates with broad branches (P1c), and stellar crystals with broad arms (P1d). The coefficients A_v (Fig. 5a) exhibit the following behavior: slow decrease to $D \sim 100$ μm, faster decrease to $D \sim 1000$–2000 μm and then asymptoting at larger values of *D*. The jump around 100 μm may be caused by intensification of the accretion processes at these sizes that influences *m–D* relations, leading to a sharp decrease of α for $D > 100$ μm (Table 1) or by the aforementioned problems with measurements or *m–D* and *A–D* parameterization in various size regions. The power indices B_v (Fig. 5b) are almost constant to the same size $D \sim 100$ μm, and then decrease quasi-exponentially for larger sizes. Figures 4b and 5b show that $B_v \sim 1$ and $V_t \sim D$ (intermediate regime when both viscous and inertial forces are important) in the size range from 40 to 300 μm, and $B_v \leq 0.5$ and $V_t \sim D^{1/2}$ (aerodynamic regime when only inertial forces are important) in the size range $D > 500$ μm; these figures illustrate how this balance of forces depends on the crystal shape.

Figure 6 compares the terminal velocity of hexagonal plates as determined from the new formulation using Mitchell's (1996) *m–D* and *A–D* relations (Table 1), the formulation of Mitchell (1996), and the data of Heymsfield and Kajikawa (1987; hereafter HK87). Comparison shows good agreement with Mitchell's parameterization below $D = 500$ μm, and values of V_t at $D > 500$ μm that are slightly larger than Mitchell (1996) with maximum difference of 25% at $D = 3000$ μm. The fit from HK87, $V_t = 297D^{0.86}$, gives values that are smaller than both theoretical curves and, being extended to larger values of *D*, are in between and close to both of the theoretical curves. Note that a comparison with HK87 may serve only as an approximate illustration since the *m–D* relations are different in Mitchell (1996; $\alpha = 0.739 \times 10^{-2}$, $\beta = 2.45$) and in HK87 ($\alpha = 3.76 \times 10^{-2}$, $\beta = 3.31$), and the *A–D* relations are absent in HK87. A more complete comparison requires simultaneous measurements of *m–D* and *A–D* relations along with V_t. Thus, collection of additional data and their analysis are needed to clarify the values of V_t for hexagonal plates.

Figure 7 shows the wide spread of the fall velocities for different crystal habits. For $D > 100$ μm, there are substantial differences in terminal velocities for the different crystal habits, which can exceed a factor of 3. These results are in general agreement with those given by Mitchell (1996), although his values are 10%–20% smaller as was in the case with hexagonal plates.

To further evaluate the new formulation for terminal velocities against experimental data, we compare the

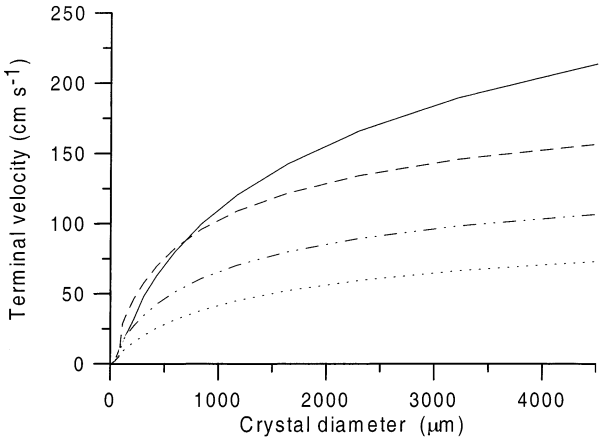

FIG. 7. Comparison of the calculated terminal velocities under standard atmospheric conditions, for various crystal habits: hexagonal columns (solid), plate with sector branches (dot), plate with broad branches (dash–dot–dot), and stellar dendrites (dash).

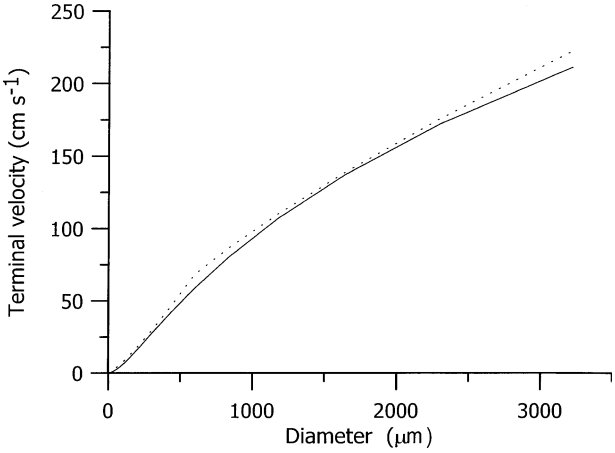

FIG. 8. Comparison of the calculated (solid) terminal velocities for bullet rosettes with observations (dot) from Heymsfield and Iaquinta (2000).

calculated values with the theoretical formulation by Heymsfield and Iaquinta (2000), $V_t = 2150D^{1.225}$ for $D < 0.06$ cm and $V_t = 492D^{0.7}$ for $D > 0.06$ cm, based on their observations for bullet rosettes (Fig. 8). There is an excellent agreement of the calculated with the observed values. Although we used Mitchell's (1996) α–σ coefficients that were obtained for the size range 200–1000 μm, this agreement may indicate that Mitchell's *m–D* and *A–D* relations are valid over the wider size range.

An additional comparison of the calculated values with experimental data is given in Fig. 9, where calculated values are compared with observations parameterized by Locatelli and Hobbs (1974) for rimed columns as $V_t = 110D^{0.56}$ and for densely rimed dendrites (R2b) as $V_t = 62D^{0.33}$. The α–σ parameters in calculations here for the dendrites are taken from LH74 (as in Mitchell 1996), and for the columns are taken from Mitchell (1996) (Table 1). It is seen from Fig. 9 that agreement is satisfactory for the columns, but the calculated V_t values for dendrites are almost twice larger than the LH74 data. This may be caused by the incorrect α–σ parameters. To test the sensitivity of V_t to uncertainty in the *m–D* and *A–D* relationships and their impact on calculated terminal velocities, we examined different values of α. The value of α used in Fig. 9 for columns (called hereafter ''old'') is $\alpha = 0.001\ 45$ (Mitchell 1996), and the new value is $\alpha = 0.001\ 25$. For dendrites, the old α derived in Mitchell from LH74 is 0.0030, and we tested a new value of $\alpha = 0.0015$. Figure 9 shows that the new values of α provide much better agreement with the observational data from LH74. This example illustrates that this method of evaluation of fall velocities can provide guidance for determining the parameters of *m–D* and *A–D* relations by fitting to the observed particles fall speeds.

4. Discussion

Based on the previous works of Abraham (1970), Bohm (1989, 1992), Mitchell (1996), and Heymsfield and Iaquinta (2000), we have derived a representation for the terminal velocities of drops and crystals as power laws, with the coefficients and indices being continuous over the entire size spectrum. The results of this work can be used in a variety of applications that are described in the following.

a. Cloud models with explicit microphysics

Cloud models with explicit microphysics usually utilize the bin representation of the particle size spectra

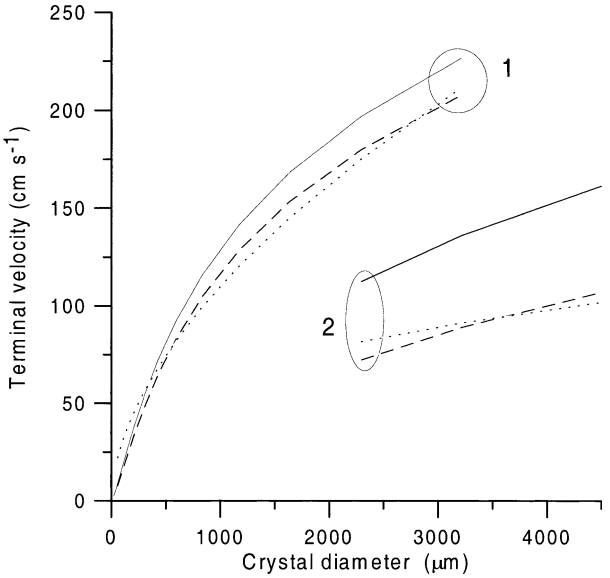

FIG. 9. Comparison of the terminal velocities for rimed dendrites 2) and rimed columns 1), using the old (solid) and new (dash) coefficients (see text) and the data of LH74 adapted by Mitchell (1996; dot). The *A–D* relations are from Mitchell (1996).

(e.g., Khvorostyanov and Sassen 1998; Gu and Liou 2000) with the particles in each bin falling at their own velocities. The boundaries of the bin positions may change with time in some models if the growth of individual drops or crystals is tracked. So, the present formulation is convenient for such models, and may give higher accuracy when using the finite-difference schemes based on the flux derivatives $d(fV_t)/dD$ or $d(fV_t)/dm$, as discussed in the introduction.

b. Cloud models with bulk microphysics

Many of the bulk microphysical parameterizations employed in cloud models use terminal velocities averaged over size spectra that are parameterized as gamma distributions or exponential functions with the parameters λ_i dependent upon the various simulated mixing ratios: rain, snow, etc. (e.g., Starr and Cox 1985; Cotton and Anthes 1989). Then V_t either is expressed analytically via λ_i, or it is evaluated numerically by integration over the parameterized size spectrum. This operation can be performed in a model at each time step or once in several steps, and the method of evaluation of V_t described here can be used effectively for each category of the bulk water and size range.

c. Regional and general circulation models

The most advanced general circulation models are beginning to use cloud microphysical parameterizations that are similar to the bulk parameterizations used in cloud models (e.g., Fowler et al. 1996, hereafter FRR96). However, the long integration periods and the large number of the grid points impose strong limitations on the number of arithmetic operations per time step, therefore some simple parameterizations are desired for GCMs rather than integration over the size spectra at each time step.

Such a simple parameterization is easily developed using the continuous representation of fall velocity that has been developed here. This parameterization is illustrated using the FRR96 bulk microphysics parameterization. The size spectrum of rain is approximated by FRR96 with the Marshall–Palmer distribution,

$$N_{DR} = N_{0R} \exp(-\lambda_R D_R), \tag{4.1}$$

where D_R is the diameter of a raindrop, $N_{0R} = 8 \times 10^2$ cm^{-4} is the intercept, $\lambda_R = (\pi\rho_w N_{0R}/\rho_a q_r)$ is the slope, and q_r is the rainwater mixing ratio. The fall velocity of a raindrop is approximated by an expression based on the Gunn–Kinzer (1949) data,

$$V_R(D_R) = (-0.267 + 5.15 \times 10^3 D_R - 1.0225 \times 10^6 D_R^2 + 7.55 \times 10^7 D_R^3)(p_0/p)^{0.4}, \tag{4.2}$$

and the average fall velocity is defined as the mass-weighted value,

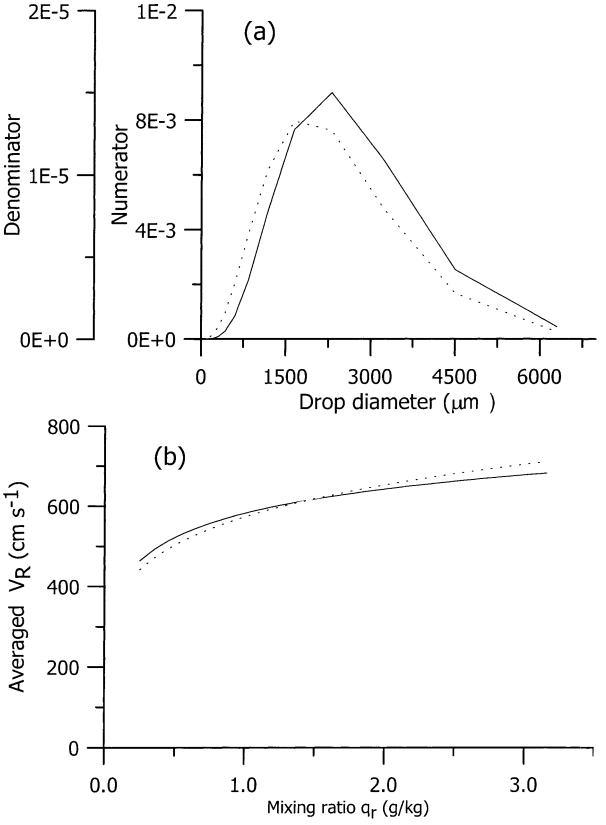

FIG. 10. (a) Subintegral functions in numerator (solid) and denominator (dot) of the average velocity (4.3); (b) a comparison of V_R calculated with the old Eq. (4.4) (solid) and new (4.5) with $c_v = 2.9$ (dot) for surface pressure.

$$\overline{V}_R = \frac{\int_0^\infty N_{0R}(D_R) M(D_R) V_R(D_R)\, dD_R}{\int_0^\infty N_{0R}(D_R) M(D_R)\, dD_R}. \tag{4.3}$$

Substitution of (4.1) and (4.2) into (4.3) and analytical evaluation of the integrals yields

$$\overline{V}_R = (-0.267 + 206 \times 10^2 \lambda_R^{-1} - 2.045 \times 10^7 \lambda_R^{-2} - (9.06 \times 10^9 \lambda_R^{-3})(p_0/p)^{0.4}. \tag{4.4}$$

This equation is used in FRR96. It can be substantially simplified using the method developed here. First, note that the subintegral functions in numerator and denominator of (4.3) have pronounced maxima at the rather narrow range of sizes near the drop diameter $D \sim 2000$–2300 μm as shown in Fig. 10a. According to section 2, $V_R(D)$ can be presented here by the power law $V_R(D_R) = A_v D_R^{B_v}$; the coefficients at the maximum are $B_{vm} \sim 0.75$ and $A_{vm} \sim 2 \times 10^3$ cm$^{0.25}$ s^{-1} as is seen in Fig. 1. This expression for V_R [which is much simpler than (4.2)] can be substituted into (4.3) since the main contribution into the integrals comes from this region. The integral is easily evaluated analytically:

$$\overline{V}_R = c_\nu A_{\nu m} \lambda_R^{-B_{\nu m}} = c_\nu A_{\nu m} \left(\frac{\rho_a q_r}{\pi \rho_w N_{0R}} \right)^{B_{\nu m}/4}, \quad (4.5)$$

where $c_\nu = \Gamma(4.7)/\Gamma(4) = 3.7$, $\Gamma(x)$ is Euler's gamma function, and $B_{\nu m}/4 = 0.188$. This expression is valid at standard atmospheric conditions. The temperature and pressure corrections can be accounted for using (2.26), which becomes now,

$$\overline{V}_R(p, T) = c_R \overline{V}_R(p_0, T_0), \qquad c_R = \left(\frac{p_0 T}{p T_0} \right)^{0.75}, \quad (4.6)$$

The actual values of A_ν, B_ν vary slightly around the mentioned maximum in (4.3), and substitution of V_R with constant coefficients may cause an error. Hence the coefficient c_ν arising from the gamma functions should be considered as a parameter that needs some tuning; our calculations show that the value $c_\nu = 2.9$ is better than 3.7 in (4.5). A comparison of V_R values calculated with the old (4.4) (solid line) and new (4.5) with $c_\nu = 2.9$ (dashed) for the surface pressure ($p_0 = p$) is given in Fig. 10b as the functions of the mixing ratio. Both equations are in excellent agreement, the maximum error is -4.7% at the lowest q_r and 4.1% at the highest q_r. Equation (4.5) is a more universal expression for raindrop terminal velocity since the corrections for both temperature and pressure can be accounted for by (4.6).

The new parameterization (4.5) is also more economical since it contains fewer arithmetic operations, and can be recommended for use in general circulation models and bulk cloud models. A similar parameterization could be developed for ice crystals using analytical expressions for ice crystal size spectra [e.g., the parameterizations of Heymsfield and Platt (1984)] or the analytical solutions in the form of modified gamma distributions obtained in Khvorostyanov and Curry (1999b). However, this is beyond of the scope of this paper and will be considered in future work.

d. Remote sensing

In some algorithms for the measurements of vertical velocities from Doppler radars, power-law approximations of V_t are used and the ''statistical'' or average relations between A_ν and B_ν are established based on numerous calculations of $A_\nu(D)$ and $B_\nu(D)$ (e.g., Matrosov and Heymsfield 2000). The calculation of $V_t(D)$ based on stepwise representation for X may create problems because the matching points by X (when the power law changes) correspond to different points in terms of diameter. This in turn may create problems when calculating the reflectivity-weighted or mass-weighted velocities by integration of the power law for V_t of individual particles with the size spectra. The method proposed here is free of such problems, A_ν–B_ν relations and averaged velocities can be easily calculated by integration using the continuous analytical form of $A_\nu(D)$ and $B_\nu(D)$ (2.24), (2.25) for the various particles types. A comparison of the calculated values of A_ν and B_ν for hexagonal columns and bullet rosettes with the fit from Matrosov and Heymsfield (2000) for bullet rosettes (Fig. 11) shows a good agreement. Note that when evaluating the integrals for the reflectivity-weighted velocities, again, the same analysis of the subintegral functions described in section 4c, above, can be performed, which can simplify the final expressions.

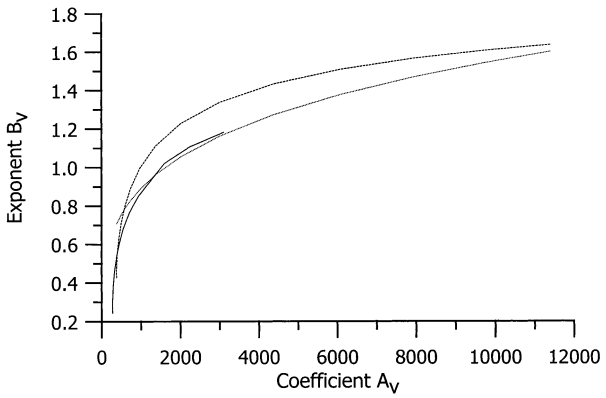

FIG. 11. A comparison of A_ν–B_ν relationships calculated with (2.24), (2.25) for hexagonal columns (solid) and bullet rosettes (dash) with the fit from Matrosov and Heymsfield (2000) for bullet rosettes (dot).

e. Other applications

In sections 2 and 3 we considered falling drops and ice crystals in air. However, the equations derived in section 2 are general and can be applied to any fluid and body by including the appropriate density of the fluid ρ_F, and density of the body ρ_b. Additional examples of falling bodies include falling dust particles in the air ($\rho_F = \rho_a$, $\rho_b = \rho_s$, with ρ_s being density of the solid material), and sinking sand particles in the ocean ($\rho_F = \rho_w$, $\rho_b = \rho_s$). In these cases $\rho_s > \rho_F$, and the velocity in (2.20)–(2.20b) is directed downward. Examples of rising bodies (with $\rho_b < \rho_F$) include the rising radiosonde balloon in the atmosphere ($\rho_F = \rho_a$, and ρ_b is the average density of the device), and the rising of frazil ice particles formed in the supercooled ocean mixed layer ($\rho_F = \rho_w$ and $\rho_b = \rho_i$). All of these situations and many other cases can be considered with (2.20a)–(2.20c).

These equations are characterized by a useful similarity criterion,

$$Y\left(\frac{\text{object}}{\text{fluid}} \right) = \nu_F^{1-2b_{\text{Re}}} \left(g \left| \frac{\rho_b}{\rho_F} - 1 \right| \right)^{b_{\text{Re}}}, \quad (4.7)$$

which is independent of the particle dimension but which does depend on the general properties of the fluid (ρ_F, ν_F), the object (ρ_b), and the planet (g). From the

definition (4.7) and (2.20c), it follows that for the ellipsoids,

$$V_t = a_{\mathrm{Re}}[(4/3)\xi(D)]^{b_{\mathrm{Re}}} D^{(3b_{\mathrm{Re}}-1)} Y(\text{object/fluid}), \quad (4.8)$$

or $V_t \sim Y$ for the particles of the same size. Thus Y allows establishment of simple similarity relations among the velocities of the falling or ascending objects in various media and planets. Consider sedimenting small dust particles in the ocean. Then in (4.7), $\rho_b = \rho_s \approx 1.5$ g cm^{-3}, $\rho_F = \rho_w = 1$ g cm^{-3}, $b_{\mathrm{Re}} = 1$, and $Y(\text{sand/water}) = (1/2)(g/\nu_w)$. For small drops in the air, $Y(\text{drop/air}) \approx (g/\nu_a)\ (\rho_w/\rho_a)$. Using for $T = 5$°C the values $\nu_w = 0.015$ cm^2 s^{-1}, and $\nu_a = 0.15$ cm^2 s^{-1}, we find that $(\nu_a/\nu_w) \sim 10$, and $(\rho_a/\rho_w) \sim 10^{-3}$, then $Y(\text{sand/water})/Y(\text{drop/air}) = (1/2)(\nu_a/\nu_w)(\rho_a/\rho_w) \approx 0.5 \times 10^{-2}$. Thus the fall speeds of the small sand particles in water is only half a percent of the value for the drops of the same radius in air. So a cloud of hydrosol particles can be transported by the ocean currents over the distances by two orders of magnitude greater than a cloud of an aerosol of the same size in the atmosphere.

5. Summary and conclusions

This paper has presented a unified treatment of cloud particle fall velocities for both liquid and crystalline cloud particles over the entire size range observed in the atmosphere. The fall velocity representation is formulated in terms of the Best (or Davies) number X, and the Reynolds number Re. For the power-law representations used in many applications, the coefficients are found as the continuous analytical functions of X (or diameter) over the entire hydrometeors size range. The advantage of the new representation of fall velocities over previous representations is that the use of continuous coefficients avoids inaccuracies at the points of discontinuity for different size regimes, allows easier parameterization of the hydrometeor size spectra, and allows continuous integration over the size spectrum.

The new formulation is compared with experimental data and previous formulations for small drops, large nonspherical drops, and various ice crystal habits. For ice crystals, published mass–dimension and area–dimension relationships are used. The new formulation was evaluated by comparing with observational data and previous formulations of the fall velocity. Evaluations of ice particle fall velocities are hampered by the lack of fall velocity data concurrent with the crystal m–D and A–D relations for the various crystal types. Existing data on crystal m–D and A–D relations for the various crystal types are still scarce and sometimes contradictory in different sources. Further collection and analysis of the data along with the parameterization of m–D and A–D relations as continuous functions of D in the entire crystal size region are needed to find the most typical values that could be recommended for use in the cloud and climate models.

Acknowledgments. This research was funded by the Department of Energy Atmospheric Radiation Measurement Program. We would like to thank A. Heymsfield, K. Sassen, J. Mace and the anonymous reviewer for their comments.

APPENDIX

List of symbols

A	maximum projected cross-sectional area
A_t	total projected area of an assembly of a body and its boundary layer
A_ν	coefficient in the velocity power law
a_{Re}	coefficient in the X–Re relation (2.9)
b_{Re}	power index in the X–Re relation (2.9)
B_ν	power index in the velocity power law
C_D	the drag coefficient
$C_0 = 0.29$	drag coefficient for potential flow
$c_1 = 0.0902$	constant in Eq. (2.8)
c_{pT}	pressure and temperature correction to the fall velocity
D	particle diameter or maximum length
D_{sc}	critical diameter that separates potential and aerodynamic flows
F_D	the drag force
F_{D0}	the drag force in a potential flow
F_b	the buoyancy force
g	the acceleration of gravity
k_1, k_2, k_3	coefficients in the empirical power law for drops
m	mass of a drop or a crystal
mg	the gravitational force
N_{0R}	the intercept of the Marshall–Palmer distribution
Re	the Reynolds number
r	droplet or crystal radius
V_R	the parameterized fall velocity in (4.2)
V_t	terminal velocity
v_b	the body volume
X	Best (or Davies) number
X_{sc}	critical Best number that separates potential and aerodynamic flows
$Y(\text{object/fluid})$	similarity parameter for the fall velocities
α	coefficient in mass–dimension relation (2.21)
β	power index in mass–dimension relation (2.21)
$\Gamma(x)$	the Euler's gamma function
γ	coefficient in area–dimension relation (2.21)
δ	the boundary layer depth
$\delta_0 = 9.06$	coefficient in the similarity relation for the boundary layer depth δ
η	the fluid dynamic viscosity

$\nu = \eta/\rho_F$	the fluid kinematic viscosity
λ_R	the slope of the Marshall–Palmer distribution
$\xi(D)$	the axes ratio of an ellipsoid
ρ_a, ρ_i, ρ_w,	the densities of air, ice, and water
ρ_b, ρ_F,	the densities of the body and fluid
σ	power index in area–dimension relation (2.21)

REFERENCES

Abraham, F., 1970: Functional dependence of drag coefficient of a sphere on Reynolds number. *Phys. Fluids,* **13,** 2194–2195.

Bashkirova, T. A., and T. A. Pershina, 1964: On the mass of snow crystals and their fall velocity. *Proc. Main Geophys. Obs.,* **165,** 83–100.

Beard, K. V., 1976: Terminal velocity and shape of cloud and precipitation drops aloft. *J. Atmos. Sci.,* **33,** 851–864.

Bohm, J. P., 1989: A general equation for the terminal fall speed of solid hydrometeors. *J. Atmos. Sci.,* **46,** 2419–2427.

——, 1992: A general hydrodynamic theory for mixed-phase microphysics. Part I: Drag and fall speeds of hydrometeors. *Atmos. Res.,* **27,** 253–274.

Cotton, W. R., and R. A. Anthes, 1989: *Storm and Cloud Dynamics.* Academic Press, 883 pp.

Fowler, L. D., D. A. Randall, and S. A. Rutledge, 1996: Liquid and ice cloud microphysics in the CSU general circulation model. Part I: Model description and simulated microphysical processes. *J. Climate,* **9,** 489–529.

Gu, Yu., and K. N. Liou, 2000: Interactions of radiation, microphysics, and turbulence in the evolution of cirrus clouds. *J. Atmos. Sci.,* **57,** 2463–2479.

Gunn, R., and G. D. Kinzer, 1949: The terminal velocity of fall for water droplets in stagnant air. *J. Meteor.,* **6,** 243–248.

Heymsfield, A. J., 1972: Ice crystal terminal velocities. *J. Atmos. Sci.,* **29,** 1348–1357.

——, and C. M. R. Platt, 1984: A parameterization of the particle size spectrum of ice clouds in terms of the ambient temperature and the ice water content. *J. Atmos. Sci.,* **41,** 846–855.

——, and M. Kajikawa, 1987: An improved approach to calculating terminal velocities of plate-like crystals and graupel. *J. Atmos. Sci.,* **44,** 1088–1099.

——, and J. Iaquinta, 2000: Cirrus crystal terminal velocities. *J. Atmos. Sci.,* **57,** 916–938.

Jayaweera, L. O. L. F., and R. E. Cottis, 1969: Fall velocities of plate-like and column ice crystals. *Quart. J. Roy. Meteor. Soc.,* **95,** 703–709.

Khvorostyanov, V. I., and K. Sassen, 1998: Cirrus cloud simulation using explicit microphysics and radiation. Part I: Model description. *J. Atmos. Sci.,* **55,** 1808–1821.

——, and J. A. Curry, 1999a: Toward the theory of stochastic condensation in clouds. Part I: A general kinetic equation. *J. Atmos. Sci.,* **56,** 3985–3996.

——, and ——, 1999b: Toward the theory of stochastic condensation in clouds. Part II: Analytical solutions of gamma distribution type. *J. Atmos. Sci.,* **56,** 3997–4013.

Lin, R.-F., D. O'C. Starr, P. J. DeMott, R. Cotton, E. Jensen, and K. Sassen, 2000: Cirrus parcel model intercomparison project phase 1. *Proc. Int. Cloud Physics Conf.,* Reno, NV, IPCC, 1221–1224.

Litvinov, I. V., 1956: Determination of falling velocity of snow particles. *Izv. Acad. Sci. USSR, Geophys. Ser.,* **7,** 853–856.

Locatelli, J. D., and P. V. Hobbs, 1974: Fall speeds and masses of solid precipitation particles. *J. Geophys. Res.,* **79,** 2185–2197.

Magono, C., and C. V. Lee, 1966: Meteorological classification of natural snow crystals. *J. Fac. Sci. Hokkaido Univ.,* **2,** 321–362.

Matrosov, S. Y., and A. J. Heymsfield, 2000: Use of Doppler radar to assess ice cloud particle fall velocity-size relations for remote sensing and climate studies. *J. Geophys. Res.,* **105,** 22 427–22 436.

Miller, S. O., and G. L. Stephens, 2001: CloudSat instrument requirements as determined from ECMWF forecasts of global cloudiness. *J. Geophys. Res.* **106,** 713–733.

Mitchell, D. L., 1994: A model predicting the evolution of ice particle size spectra and radiative properties of cirrus clouds. Part I: Microphysics. *J. Atmos. Sci.,* **51,** 797–816.

——, 1996: Use of mass- and area-dimensional power laws for determining precipitation particle terminal velocities. *J. Atmos. Sci.,* **53,** 1710–1723.

——, and W. P. Arnott, 1994: A model predicting the evolution of ice particle size spectra and radiative properties of cirrus clouds. Part II: Dependence of absorption and extinction on ice crystal morphology. *J. Atmos. Sci.,* **51,** 817–832.

Petch, J. C., G. C. Craig, and K. P. Shine, 1997: A comparison of two bulk microphysical schemes and their effects on radiative transfer using a single-column model. *Quart. J. Roy. Meteor. Soc.,* **123,** 1561–1580.

Pruppacher, H. R., and J. D. Klett, 1997: *Microphysics of Clouds and Precipitation.* Kluwer, 997 pp.

Rogers, R. R., 1976: *A Short Course in Cloud Physics.* A. Wheaton & Co., 266 pp.

Starr, D. O'C., and S. K. Cox, 1985a: Cirrus clouds. Part I: A cirrus cloud model. *J. Atmos. Sci.,* **42,** 2663–2681.

——, and ——, 1985b: Cirrus clouds. Part II: Numerical experiments on the formation and maintenance of cirrus. *J. Atmos. Sci.,* **42,** 2682–2694.

——, and Coauthors, 2000: Comparison of cirrus cloud models: A project of the GEWEX Cloud System Study (GCSS) working group on cirrus cloud systems. *Proc. Int. Cloud Physics Conf.,* Reno, NV, IPCC, 1–4.